Systematics of reaction cross sections and interaction barriers for charged particles*

Louis C. Vaz and John M. Alexander
Department of Chemistry, State University of New York at Stony Brook, Stony Brook, New York 11794
(Received 27 December 1973)

Experimentally determined total reaction cross sections σ_R have been used to obtain the systematics of interaction barriers in reactions between charged nuclei. The real potential was assumed to be parabolic at its maximum and hence the characteristic parameters are barrier height, radius, and curvature, E_0, R_0, and $\hbar\omega_0$, respectively. Barrier heights and radii follow clear systematic trends and therefore these systematics can be used to predict total reaction cross sections for energies close to and greater than the barrier. Experimental data for incident energies below the barrier are sparse and therefore they cannot be well systematized at this time. The cross section patterns for low incident energies seem to reflect individuality of the collision partners.

[NUCLEAR REACTIONS Total cross sections σ_R for charged particle reactions are systematized in terms of a real inverted parabolic barrier. Graphical interpolation and extrapolation of the interaction barrier E_0 permit prediction of σ_R.]

I. INTRODUCTION

Through the years a rather substantial body of experimental information has been obtained on total reaction cross sections in charged particle reactions. A variety of models has been used to correlate and/or calculate the total reaction cross section σ_R.[1-7] The parameters of these models have been deduced by reference to experimental data, usually from studies of elastic scattering[1,8,9] and in some cases from reaction cross sections.[2-5] However, if one calculates σ_R according to the various prescriptions[1,2,4,5,10] that have been given, one obtains quite divergent results, especially for energies near the interaction barrier. This situation seems to arise from two independent sources: (1) the models themselves and (2) the systemization of the parameters of the models.

The simplest model used is that of two sticky hard spheres (charges Z_1e and Z_2e) that obey classical mechanics. The total reaction cross section σ_R in this case is given by the equation

$$\sigma_R = \pi R^2[1 - V(R)/E], \tag{1}$$

where R denotes the distance between centers of the two spheres at contact, $V(R)$ is the potential energy of the spheres, often taken to be $V(R) = Z_1Z_2e^2/R$, and E is the collision energy in the center of mass frame. A reasonably precise approximation to σ_R for ions of He and heavier is given by $R = 1.5(A_1^{1/3} + A_2^{1/3})$ fm.[10] As Eq. (1) does not allow for barrier penetration, one expects its usefulness to be limited to energies significantly greater than the interaction barrier $[E > 1.2V(R)]$.

An optical potential with real and imaginary parts can provide σ_R values below and above the barrier. Effects of both penetrability and transparency are contained in such a potential. Very good fits to elastic scattering[1,9] and reaction cross sections[1-6] have been obtained. However, for heavier projectiles there are ambiguities in the parameter choices which make it difficult either to obtain a unique set of parameters or to extrapolate to new reaction systems.[1,11] Also, the effects of deformation of either reaction partner are difficult to include. For the description of σ_R for heavier projectiles at moderate energies the most important feature of the potential seems to be the real part near its maximum.[7] Therefore, a parametrization of the potential that focuses our attention here is most apt to reveal simple systematic variations.

The very simple approximation of a real parabolic potential (for energies near the barrier maximum) has been used rather often in this context. The imaginary potential is taken implicitly to be large in the nuclear interior and negligible on the outer surface. Such a representation clearly cannot describe transparency but for strongly absorbed particles (heavier ions at moderate energies) it provides a simple basis for examining systematic variations. The inverted parabola is a stand-in for the combined effects of Coulomb repulsion and nuclear attraction.[12] Recently Wong[7] has used this parabolic barrier approximation to obtain a very simple expression for the total reaction cross section. Wong's expression has three parameters, the interaction energy (E_0) for $l = 0$, the interaction radius (R_0) corresponding to the top of the potential, and the curvature ($\hbar\omega_0$ in MeV) of the potential. It includes penetrability in a manner that should be reasonably accurate near the

barrier. The treatment can be rather easily modified to approximate the effects of small deformation(s) of the reaction partner(s).

We have been attracted to the parabolic barrier approximation for several reasons: (1) the simplicity of the potential (three parameters for spherical reactants, four for deformed), (2) the explicit statement of the barrier maximum in the potential parametrization, (3) the inclusion of penetrability and deformation in a simple fashion, and (4) the expectation that the parameters can be extrapolated to new reaction systems. We have used experimental determinations of reaction cross sections to fix the three independent parameters. At present the effects of penetrability and deformation cannot be resolved, but the semiempirical parameters could conceivably separate these effects if better data are obtained. The very important interaction barrier has been systematized graphically to allow interpolation or extrapolation for any desired reaction partners. Estimates of total reaction cross sections and their uncertainties can be made from the quality of fit to existing results and the scatter in the correlation of the parameters. As new experiments are performed the empirical parameters can be easily modified.

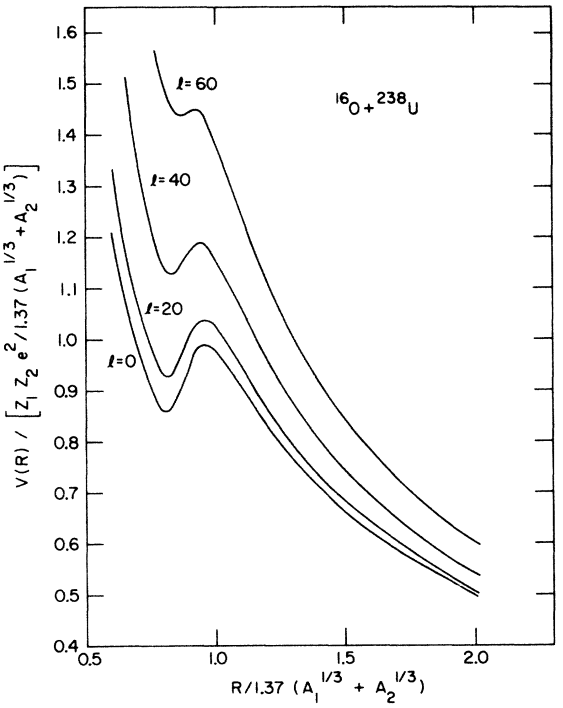

FIG. 1. Effective potential $V(R) = V_N(R) + V_C(R) + V_{CF}(R)$ for various partial waves. The nuclear potential $V_N(R) = V_0/\{1 + \exp[R - r_0(A_1^{1/3} + A_2^{1/3})]/a\}$ with $V_0 = -40.0$ MeV, $a = 0.50$ fm, and $r_0 = 1.2$ fm. The Coulomb potential $V_C(R) = Z_1 Z_2 e^2/R$. The centrifugal potential $V_{CF}(R) = l(l+1)\hbar^2/2\mu R^2$. The values of R_l for $l = 0$, 20, 40, and 60, are 11.50, 11.40, 11.20, and 10.90 fm, respectively. Similarly, values of $\hbar\omega_l$ are 5.51, 5.76, 5.98, and 5.26 MeV, respectively.

II. PARABOLIC BARRIER

Wong[7] has derived the following expression for the reaction cross section for penetration of a spherical parabolic potential:

$$\sigma_R = \left(\frac{R_0^2}{2}\right)\left(\frac{\hbar\omega_0}{E}\right)\ln\{1 + \exp[2\pi(E - E_0)/\hbar\omega_0]\}. \tag{2}$$

The parameters R_0, E_0, and $\hbar\omega_0$ are the radius, height, and curvature of the parabolic potential barrier for s waves. Penetration of this real potential barrier is identified with absorption. The expression reduces to the form of Eq. (1) for $2\pi(E - E_0)/\hbar\omega_0 \gg 1$. Tunneling is included by the use of the Hill-Wheeler formula[13] for the penetration coefficient $P(l, E)$ for the partial wave l,

$$P(l, E) = \{1 + \exp[2\pi(E_l - E)/\hbar\omega_l]\}^{-1}, \tag{3}$$

where

$$E_l = V_N(R_l) + V_C(R_l) + \hbar^2 l(l+1)/2\mu R_l^2 \tag{4}$$

and the corresponding curvature is defined by

$$\hbar\omega_l = [\hbar^2 V''(R_l)/\mu]^{1/2}, \tag{5}$$

where $V''(R_l)$ denotes $|\partial^2 V(R)/\partial R^2|_{R_l}$. Symbols

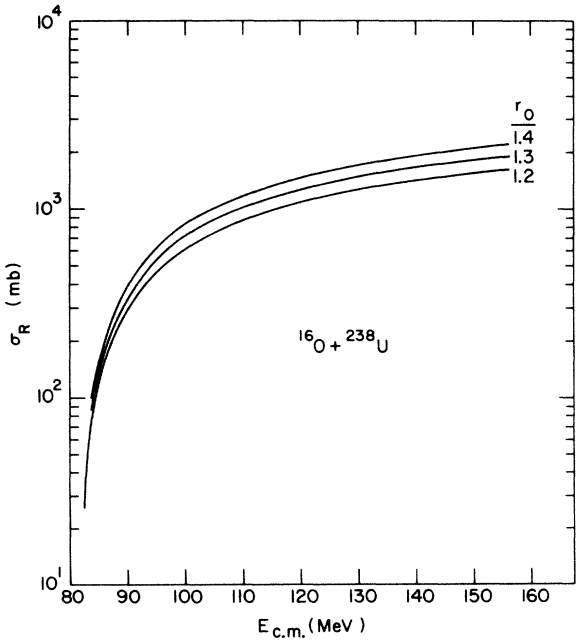

FIG. 2. Calculated curves for σ_R vs E from Eq. (2) for various values of r_0 (fm). The parameters E_0, $\hbar\omega_0$, and Δ were 82.15 MeV, 4.0 MeV, and zero, respectively.

R_l, E_l, and $\hbar\omega_l$ denote the radial distance, height, and curvature, respectively, of the barrier against the lth partial wave. The quantity V denotes potential energy with subscripts N for nuclear and C for Coulomb potential, respectively. The simplicity of Eq. (2) arises from the approximation that the radial distance R_l and curvature of the potential at its maximum $\hbar\omega_l$ are both independent of l (i.e., $R_l \approx R_0$ and $\hbar\omega_l \approx \hbar\omega_0$). Figure 1 shows the real part of an effective potential $V(R)$ for one choice of parameters and several different l values for the system $^{238}U + ^{16}O$. Wong's approximations ($R_l \approx R_0$ and $\hbar\omega_l \approx \hbar\omega_0$) seem to be justified for this case.

Equation (2) thus provides a three parameter relationship to describe the energy dependence of σ_R. The sensitivity of the relationship to each parameter is shown in Figs. 2–4. The quantity R_0^2 is simply a multiplicative factor and is most easily determined from σ_R values at high energies ($E \gg E_0$). The quantity $\hbar\omega_0$ is important only for low energies ($E \lesssim E_0$) where data are, in fact, very sparse. The quantity E_0 is very important for the shape of the excitation function at low to intermediate energies, but is unimportant for rather high energies ($E \gg 2E_0$).

A typical fit to experimental data[6] is shown in Fig. 5. Comparison of Figs. 2–4 with Fig. 5 indicates that the experimental results are generally not numerous enough at low energies to fix $\hbar\omega_0$ but that both E_0 and R_0 can be determined to a few percent.

The derivation of Eq. (2) has neglected nuclear deformation (both static and dynamic). Wong[7] has modified the treatment so that very small static deformations can be included as a perturbation. His treatment involves a series expansion that we feel is not appropriate for the large deformation parameters ($\beta > 0.1$) often encountered.[7] We have chosen to approximate deformation effects by considering the interaction barrier E_0 to have a uniform distribution of values between $\overline{E}_0 - \Delta$ and $\overline{E}_0 + \Delta$. The physical meaning of this approximation is that l is retained as a good quantum number and the interaction barrier is said to be raised or lowered uniformly by the various angles of the nuclear symmetry axis (axes). Wong's treatment also retains l as a good quantum number, but he obtains the spectrum of barrier heights from the electrostatic repulsion between nuclear quadrupoles with random orientations.[7] In Fig. 6 the real part of an effective potential is shown between ^{16}O and ^{238}U ($\beta_{22} = 0.277$, Ref. 14) for the extreme angular orientations of the symmetry axis.[15] These potential energy curves are compared to those obtained for the same potential with $\beta_{22} = 0$. From Fig. 6 one might expect the deformation parameter $\beta_{22} = 0.277$ to result in a distribution of E_0 val-

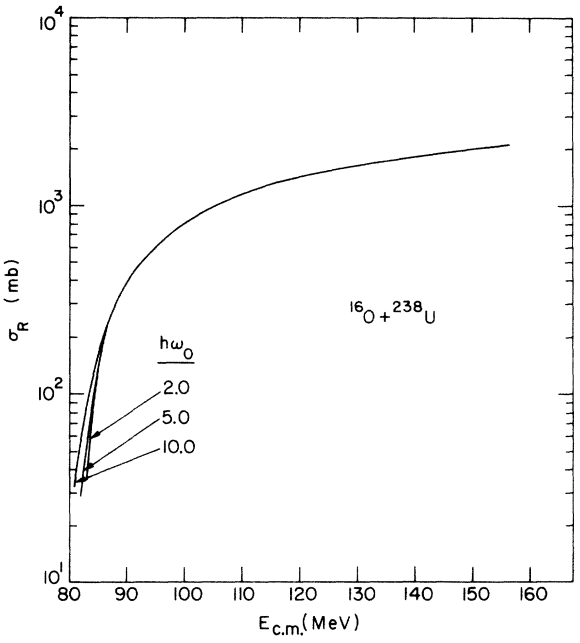

FIG. 3. Calculated curves for σ_R vs E from Eq. (2) for various values of $\hbar\omega_0$ (MeV). The parametrs r_0, E_0, and Δ were 1.37 fm, 82.15 MeV, and zero, respectively.

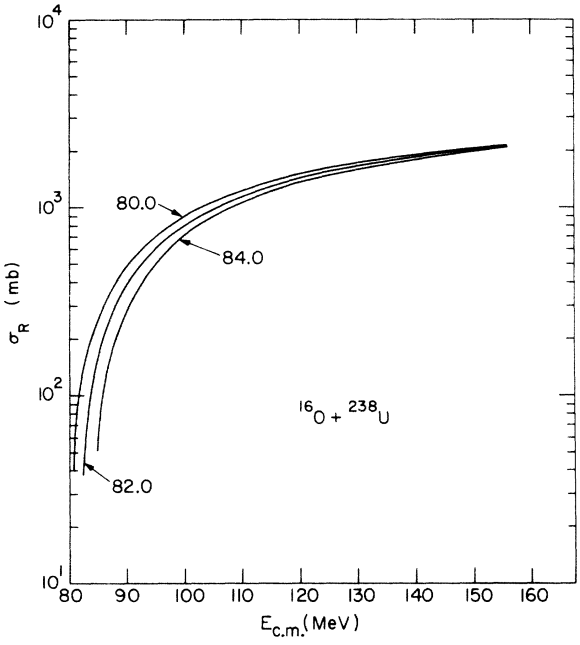

FIG. 4. Calculated curves for σ_R vs E from Eq. (2) for various values of E_0 (MeV). The parameters r_0, $\hbar\omega_0$, and Δ were 1.37 fm, 4.0 MeV, and zero, respectively.

ues with $\Delta \approx 3$ MeV and possibly a lowering of $\overline{E}_0$ compared to the case for $\beta_{22}=0$. However, the dynamics of the collision are not included in such hasty considerations. The problem of dynamic effects in general, and for deformed nuclei in particular, has been a subject of considerable theoretical study.[4,16] Unfortunately, the comparisons of experiment with theory give us no compelling general conclusions as yet. In this work we will be led by the experimental data to assign values of Δ which provide best fits. One may then attempt to relate the values of Δ to deformation parameters of the colliding partners.

The effect of the Δ parameter on σ_R is shown in Fig. 7. Clearly the parameters Δ and $\hbar\omega_0$ are very similar in nature and one cannot hope to determine them independently. (In fact, as will be clear later, only rarely does one have reliable data for $E<\overline{E}_0$. Therefore, values of both $\hbar\omega_0$ and Δ cannot be considered to be very well known as yet.)

We have chosen to fit calculation to experiment with $\hbar\omega_0=4.0$ MeV[17] and then search for "best values" of $\overline{E}_0$, R_0, and Δ. The values of $\overline{E}_0$ and R_0 are reduced to the radius parameters r_e and r_0, respectively:

$$\overline{E}_0 = Z_1 Z_2 e^2 / R_e \,, \tag{6}$$

with

$$R_e = r_e A_1^{1/3} + R_2 \tag{7}$$

and

$$R_0 = r_0 A_1^{1/3} + R_2 \,, \tag{8}$$

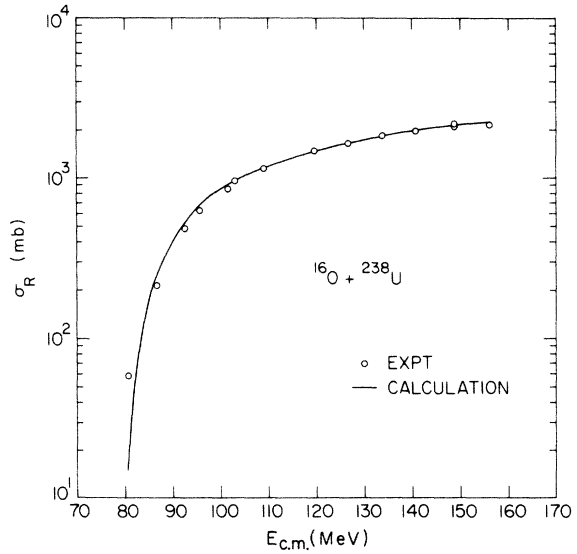

FIG. 5. Calculated curves and experimental points (Ref. 6) for $^{238}U + ^{16}O$. The best-fit parameters r_0, $\overline{E}_0$, $\hbar\omega_0$, and Δ are 1.41 fm, 82.10 MeV, 4.0 MeV, and 2.8 MeV, respectively.

where R_2 is the radius of one collision partner, as discussed later. Figure 8 summarizes the meaning of the various parameters used in the parabolic approximation and shows their magnitudes for the reaction system $^{238}U + ^{16}O$.

Information about the interaction potential has also been obtained from studies of elastic scattering. There is, of course, a wealth of data here and invariably a radius parameter is reported in the analysis. Often this radius parameter is extracted by phase shift and amplitude parametrizations such as the Blair sharp cutoff prescription.[8,18] These parametrizations may well reflect somewhat different aspects of the interaction potential from those focused on here. Therefore, we feel that a reanalysis of these data is required before both elastic scattering and reaction cross sections can be used in a self-consistent way.

The simplified potential used here is certainly not capable of capturing the energy dependence of

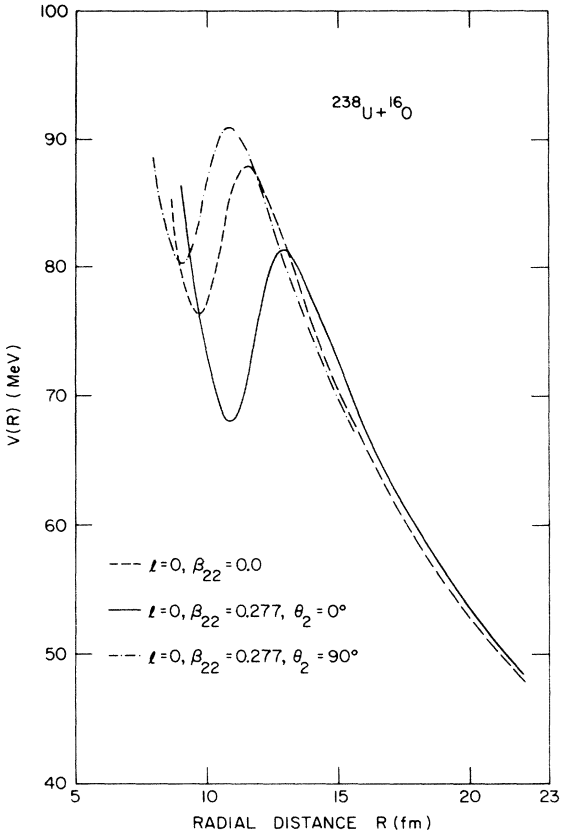

FIG. 6. Effective potential $V(R)$ for s waves for the system $^{238}U + ^{16}O$ (β_{21} for ^{16}O is assumed to be zero). [See Eqs. (12) and (13) of Ref. 7.] Parameter values are $V_0=-40.0$ MeV, $a=0.50$ fm, $r_0=1.2$ fm. The curves are as follows: (a) $\beta_{22}=0.0$, both collision partners are spheres: ---; (b) $\beta_{22}=0.277$, $\theta_2=0°$: ——; (c) $\beta_{22}=0.277$, $\theta_2=90°$: —·—.

the nuclear transparency. Measurements of proton cross sections at energies of ≳20 MeV exhibit a decrease with increasing energy—clearly revealing this important feature. For the more complex projectiles and/or lower velocities the transparency can be expected to be small. We have restricted the parameter determinations to include only such systems and similarly the application of these systematics should be limited correspondingly.

III. PROCEDURE FOR PARAMETER SEARCH

We have analyzed most of the available experimental data on total reaction cross sections measured with ^{1}H,[19-39] ^{2}H,[20,21,45-50] ^{3}He,[51] ^{4}He,[52-58] and heavy ions,[6,40-44,58] and experimental data on partial reaction cross sections.[59-77] The experimental determinations of reaction cross sections may be placed in three groups which we have treated differently: (A) Studies of the reaction cross section versus energy for one target-projectile system. (B) Studies of the reaction cross section at one or more projectile energies very high above the interaction barrier. (C) Studies of the partial reaction cross section σ_i near the barrier ($E \approx \bar{E}_0$) for a reaction system for which σ_i/σ_R is expected to be a slowly varying function of energy. Only for data in group (A) may the three potential parameters be determined independently for one reaction system. The results in group (B) are for high energies ($E > \bar{E}_0$) and therefore are most sensitive to R_0. The useful results in group (C) are for low energies ($E \approx \bar{E}_0$) and are thus most sensitive to $\bar{E}_0$. We discuss these groups in order.

A. Reaction cross section known as a function of energy

In Table I are listed the reaction systems that have been studied near and above the barrier along with the "best-fit" parameters. Studies[42-44] of σ_R that extend to very low energies are discussed later. (See Sec. IV B.) Our search for the best-fit values of $\bar{E}_0$, R_0, and Δ has been made by visual comparison of experimental and calculated values of σ_R. We have not been able to establish a clearcut objective way of weighting the individual experimental determinations, and therefore we have not used a free search routine for these fits. Many of the measurements were made with uncertain energy control for $E \approx \bar{E}_0$, and a free least-squares search would lead to some wild fluctuations in the parameters. Instead, we have obtained best fits by minimizing the systematic deviations and assigning low weight to determina-

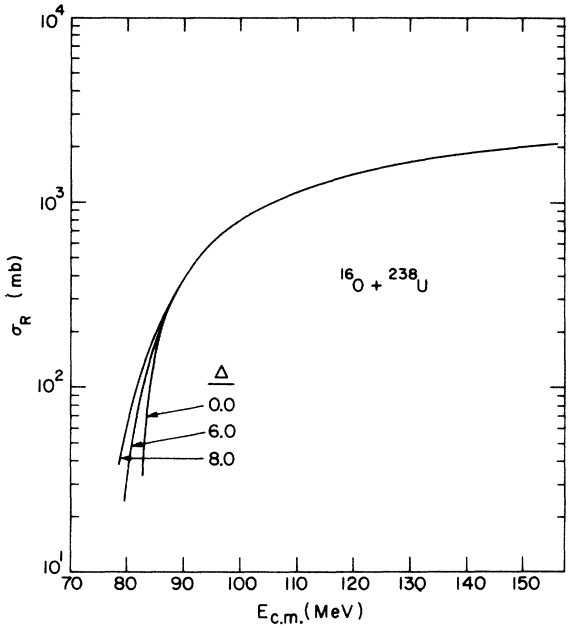

FIG. 7. Calculated curves for σ_R vs E from Eq. (2) for various values of Δ (MeV). The parameters r_0, $\bar{E}_0$, and $\hbar\omega_0$ were 1.37 fm, 82.15 MeV, and 4.0 MeV, respectively.

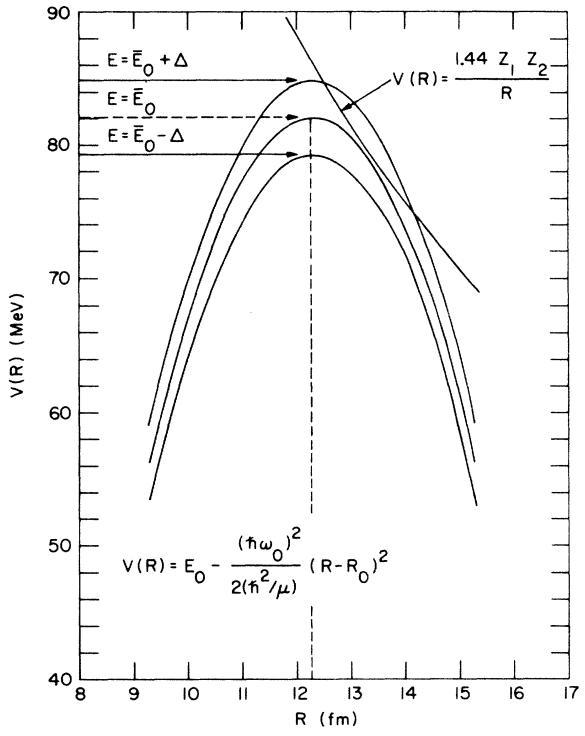

FIG. 8. Interaction barrier in the parabolic approximation with the best-fit parameters from Fig. 5. The point-charge Coulomb potential $V_C(R)$ is also shown. The spectrum of barrier heights was uniform ranging from $\bar{E}_0 - \Delta$ to $\bar{E}_0 + \Delta$. The values of $\hbar\omega_0$ and R_0 were taken as constant. See Sec. II.

TABLE I. Barrier parameters from cross sections measured at many energies.

Reaction	Z_1Z_2	$\bar{E}_0$ (MeV)	Δ (MeV)	R_e (fm)	r_e (fm)	R_0 (fm)	r_0 (fm)	Reference
$Al+{}^1H$	13	2.89	3.3	6.48	1.68	5.60	1.39	21,22,30,36,37
$^{51}V+{}^1H$	23	4.20	3.3	7.89	1.74	6.92	1.48	24,39
$Fe+{}^1H$	26	4.70	3.2	7.97	1.71	6.90	1.43	21,22,30,34,36
$Co+{}^1H$	27	4.76	3.0	8.17	1.73	7.14	1.46	21,22
$Ni+{}^1H$	28	5.15	3.0	7.83	1.64	6.70	1.35	21,36,37
$Cu+{}^1H$	29	5.05	3.2	8.27	1.71	7.15	1.43	20–23,31,33–37
$^{63}Cu+{}^1H$	29	5.00	3.2	8.35	1.74	7.32	1.48	21–26,30,39
$^{65}Cu+{}^1H$	29	4.95	3.4	8.44	1.74	7.38	1.48	21–26,30,39
$Zn+{}^1H$	30	5.10	3.2	8.47	1.74	7.33	1.46	21,22,36
$Zr+{}^1H$	40	6.20	3.0	9.29	1.75	8.08	1.48	23,36
$Ag+{}^1H$	47	6.99	3.0	9.68	1.73	8.47	1.48	21,36
$In+{}^1H$	49	7.16	3.0	9.86	1.73	8.74	1.50	21
$^{233}U+{}^1H$	92	11.60	2.6	11.42	1.62	10.59	1.49	19
$^{232}Th+{}^2H$	90	10.70	5.0	12.11	1.62	11.03	1.44	46
$^{233}U+{}^2H$	92	10.80	3.2	12.27	1.64	10.97	1.43	46
$^{238}U+{}^2H$	92	11.00	3.2	12.04	1.59	11.19	1.45	46
$^{59}Co+{}^4He$	54	8.92	2.6	8.72	1.59	8.11	1.43	52
$^{233}U+{}^4He$	184	22.00	2.8	12.04	1.55	10.91	1.36	53
$^{238}U+{}^4He$	184	22.25	2.8	11.91	1.51	10.82	1.34	6,53
$^{237}Np+{}^4He$	186	22.60	3.0	11.85	1.51	10.89	1.35	56
$^{238}U+{}^{11}B$	460	52.50	3.0	12.62	1.50	11.79	1.40	6
$^{238}U+{}^{12}C$	552	63.60	4.0	12.56	1.48	11.88	1.40	6
$^{238}U+{}^{14}N$	644	72.90	2.8	12.72	1.48	11.96	1.39	6
$^{238}U+{}^{16}O$	736	82.10	2.8	12.91	1.48	12.29	1.41	6
$^{238}U+{}^{20}Ne$	920	101.45	7.7	13.06	1.47	12.39	1.39	6
$^{238}U+{}^{40}Ar$	1656	173.45	3.5	13.75	1.43	13.37	1.39	40
$^{24}Mg+{}^{32}S$	192	28.28	3.0	9.78	1.61	8.54	1.41	41
$^{27}Al+{}^{32}S$	208	30.05	3.0	9.97	1.61	8.71	1.41	41
$^{40}Ca+{}^{32}S$	320	43.75	2.2	10.53	1.60	9.30	1.41	41

tions at the lower energies ($E \lesssim \bar{E}_0$). For essentially all systems (see Sec. IV) the calculated values of σ_R for $E \gtrsim \bar{E}_0$ are within the experimental uncertainties in the data. The deviation plots shown in Figs. 9–11 illustrate this fact.

B. Reaction cross sections at one or more energies high above the interaction barrier

Reference to Figs. 2–5 shows that the magnitude of σ_R at high energies is mainly determined by the value of R_0. However, it is obvious that Eq. (2) requires values of $\bar{E}_0$, $\hbar\omega_0$, and Δ before values of R_0 can be obtained. From the trends in Table I, as discussed in the next section, we chose values for R_e, $\hbar\omega_0$ (4.0 MeV), and Δ (3.0 MeV). Then we averaged Eq. (2) for E_0 values from $\bar{E}_0 - \Delta < E_0 < \bar{E}_0 + \Delta$ and solved for R_0. The values of R_0 are given in Table II.

Correlation of the values of R_0

In Tables I and II we have listed 136 values of R_0. We wish to reduce these values to the separate radii for target and projectile. For this purpose we use the following assumption:

$$R_0 = r_0 A_1^{1/3} + R_2 . \tag{8}$$

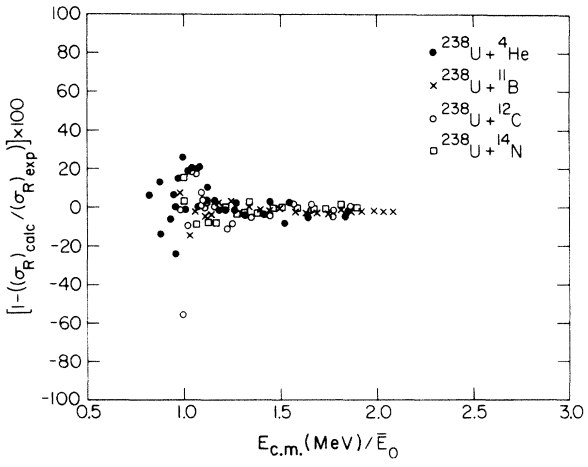

FIG. 9. Deviations between the total reaction cross sections as measured $(\sigma_R)_{exp}$ and as calculated $(\sigma_R)_{calc}$ for the reactions indicated. Data from Refs. 6 and 53.

The values of R_2 are determined as follows: For $A \geq 6$, $R_2 = r_0 A_2^{1/3}$; for ^{1}H, ^{2}H, ^{3}He, and ^{4}He separate individual values of R_2 are obtained from the measurements. We have ≈136 experimental values of R_0 from which to fix five parameters by a least-square analysis.[78] In Table III we give the values of the five radius parameters obtained and their uncertainties. In this analysis every experimental point was given an equal weight. In Fig. 12 we illustrate the behavior of $R_0 - R_2$ as a function of $A^{1/3}$. We conclude that the radius parameters in this formulation are rather well determined and that systematic deviations from Eq. (8) are not apparent over a wide mass region.[79] Significant deviations from the $A^{1/3}$ law may occur, of course, in specific regions and these are discussed in the original references.

C. Partial reaction cross sections determined near the barrier $E \approx \bar{E}_0$ (Refs. 59–77)

Reference to Figs. 2–5 shows that magnitude of σ_R near the barrier is very sensitive to the choices of $\bar{E}_0$ and, to a lesser extent, Δ. From the parameters in Table I we can expect Δ to be about 3.0 MeV for most reaction systems. Therefore, we can expect the energy dependence of σ_R near the barrier to reflect mainly the value of $\bar{E}_0$. To obtain $\bar{E}_0$ we have fixed the other parameters as follows: $\Delta = 3.0$ MeV, $\hbar\omega_0 = 4.0$ MeV, and R_0 from Eq. (8) and Table III. Over a small range of energies we can often expect (σ_i/σ_R) to be nearly constant, and we have varied $\bar{E}_0$ until this condition is obtained. In Table IV we give, for each reaction system, the energy span used in the analysis and the value of $\bar{E}_0$ obtained. The values of $\bar{E}_0$ were reduced to r_e by use of Eqs. (6) and (7). The values of R_2 for ^{1}H, ^{2}H, ^{3}He, and ^{4}He were taken from Table III, and for $A \geq 6$ we set $R_2 = r_e A_2^{1/3}$.

We have listed in Tables I–IV the values of potential energy parameters (R_0, $\bar{E}_0$, Δ, and $\hbar\omega_0$) that provide best fits to the large body of available experimental data. In the next section we discuss the systematic trends and the predictive value of these results.

IV. RESULTS AND DISCUSSION

A. Incident energies above the barrier $E \gtrsim \bar{E}_0$

As discussed in the Introduction, the intent of this work is to systematize our knowledge of total reaction cross sections. The systematics are most useful if the number of parameters employed is small and if these parameters can be easily interpolated or extrapolated for any reaction partners. With the parabolic barrier approximation, the calculated values of σ_R are mainly sensitive to $\bar{E}_0$ and R_0 for energies near to or greater than the barrier (σ_R some tens of millibarns or more). For these energies there is only small sensitivity to Δ and $\hbar\omega_0$. From the values of R_0 and $\bar{E}_0$ we have obtained the more slowly varying quantities r_0 and r_e. These two radius parameters are plotted against the product $Z_1 Z_2$ in Figs. 13 and 14. These parameters are predicted to decrease with $Z_1 Z_2$ because of the increasing Coulomb potential.[7] The trend of the experimental points is very clear indeed and is represented by the solid lines in Figs. 13 and 14. It is very difficult to assign experimental uncertainties to each point and therefore the existence of significant deviations from the solid lines is not evident. It appears that the value of r_0 (1.416 ± 0.008) is essentially independent

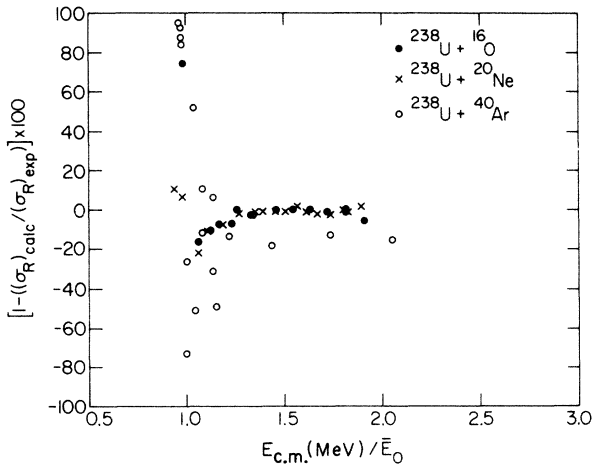

FIG. 10. Deviations between the total reaction cross sections as measured $(\sigma_R)_{exp}$ and as calculated $(\sigma_R)_{calc}$ for the reactions indicated. Data from Refs. 6 and 40.

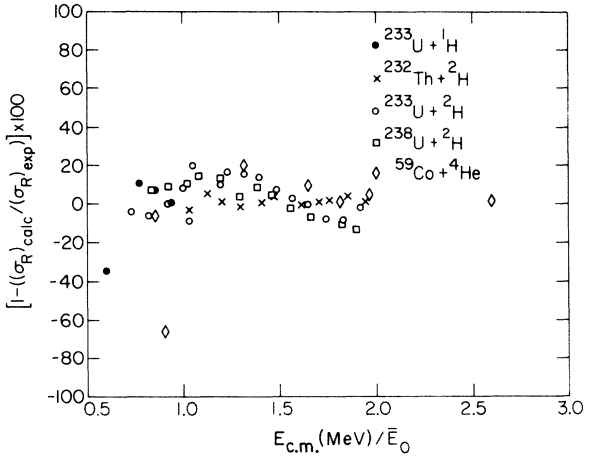

FIG. 11. Deviations between the total reaction cross sections as measured $(\sigma_R)_{exp}$ and as calculated $(\sigma_R)_{calc}$ for the reactions indicated. Data from Refs. 19, 46, and 52.

TABLE II. The parameters R_0 from cross sections measured at high energies. Proton irradiations with energies >20 MeV are not included because of the possibility of nuclear transparency.

Reaction	Z_1Z_2	R_0 (fm)	r_0 (fm)	Reference
Be + ^{1}H	4	4.31	1.38	32, 36
C + ^{1}H	6	3.75	1.01	27–29, 36, 37
Mg + ^{1}H	12	5.24	1.32	23, 37
^{40}Ca + ^{1}H	20	5.79	1.27	28, 38
^{45}Sc + ^{1}H	21	5.83	1.23	24
Ti + ^{1}H	22	6.53	1.40	23, 30, 36
^{49}Ti + ^{1}H	22	6.48	1.39	26
V + ^{1}H	23	6.78	1.44	22, 30, 31, 36
^{55}Mn + ^{1}H	25	6.87	1.43	24
^{54}Fe + ^{1}H	26	6.45	1.33	25, 26
^{56}Fe + ^{1}H	26	6.76	1.39	25, 26
^{57}Fe + ^{1}H	26	6.79	1.39	25, 26
^{58}Fe + ^{1}H	26	7.11	1.46	25, 26
^{58}Ni + ^{1}H	28	6.72	1.36	21, 22, 25, 26
^{60}Ni + ^{1}H	28	6.93	1.40	21, 22, 25, 26
^{62}Ni + ^{1}H	28	7.19	1.45	25, 26
^{64}Zn + ^{1}H	30	6.95	1.38	25, 26
^{66}Zn + ^{1}H	30	7.21	1.43	25, 26
^{68}Zn + ^{1}H	30	7.32	1.44	25, 26
Ga + ^{1}H	31	8.41	1.69	22
^{90}Zr + ^{1}H	40	7.24	1.29	26
^{91}Zr + ^{1}H	40	7.26	1.29	26
^{92}Zr + ^{1}H	40	7.61	1.37	26
^{94}Zr + ^{1}H	40	7.88	1.42	26
Nb + ^{1}H	41	8.02	1.45	36
Mo + ^{1}H	42	8.20	1.48	36
Rh + ^{1}H	45	8.70	1.55	36
Cd + ^{1}H	48	9.16	1.60	21
Sn + ^{1}H	50	8.40	1.42	36
^{116}Sn + ^{1}H	50	8.58	1.46	26
^{117}Sn + ^{1}H	50	8.54	1.45	26
^{118}Sn + ^{1}H	50	8.86	1.51	26
^{119}Sn + ^{1}H	50	8.54	1.44	26
^{120}Sn + ^{1}H	50	8.54	1.44	26
Ta + ^{1}H	73	9.59	1.44	36
Pb + ^{1}H	82	10.17	1.48	36, 37
Be + ^{2}H	4	5.41	1.55	49, 50
C + ^{2}H	6	5.71	1.54	48 [a], 49, 50
Mg + ^{2}H	12	6.55	1.51	50
Al + ^{2}H	13	6.52	1.44	49, 50
Ti + ^{2}H	22	7.34	1.42	49, 50
V + ^{2}H	23	7.65	1.47	49, 50
Fe + ^{2}H	26	7.68	1.44	49, 50
Co + ^{2}H	27	7.88	1.46	50
Ni + ^{2}H	28	7.72	1.42	20, 21 [a], 49, 50
^{58}Ni + ^{2}H	28	8.98	1.76	21, 47, 48 [a]
^{60}Ni + ^{2}H	28	9.06	1.75	21, 47, 48 [a]
Cu + ^{2}H	29	7.94	1.44	21 [a], 49, 50
^{63}Cu + ^{2}H	29	9.33	1.79	21 [a]
^{65}Cu + ^{2}H	29	9.67	1.86	21 [a]
Zn + ^{2}H	30	8.19	1.48	49, 50
Zr + ^{2}H	40	8.41	1.38	45 [a], 49, 50
Nb + ^{2}H	41	8.57	1.41	45 [a], 49
Rh + ^{2}H	45	8.92	1.44	49, 50
Ag + ^{2}H	47	8.85	1.40	49, 50
Sn + ^{2}H	50	8.71	1.33	49, 50
Ta + ^{2}H	73	9.75	1.34	49, 50
Au + ^{2}H	79	9.98	1.34	49, 50
Pb + ^{2}H	82	10.26	1.37	49, 50
Bi + ^{2}H	83	10.14	1.41	48 [a], 49
Mg + ^{3}He	24	7.01	1.22	51
Al + ^{3}He	26	7.29	1.26	51
Fe + ^{3}He	52	8.64	1.34	51
Ni + ^{3}He	56	9.12	1.44	51
Cu + ^{3}He	58	9.36	1.46	51
Ag + ^{3}He	94	11.29	1.64	51
Be + ^{4}He	8	5.21	1.29	55
C + ^{4}He	12	5.62	1.35	55, 57
Al + ^{4}He	26	6.56	1.34	55
Ti + ^{4}He	44	7.78	1.44	55
V + ^{4}He	46	7.73	1.40	55
Cr + ^{4}He	48	7.93	1.45	54
Fe + ^{4}He	52	7.90	1.40	54, 55
Co + ^{4}He	54	8.28	1.48	54
Ni + ^{4}He	56	7.95	1.39	54, 55
Cu + ^{4}He	58	8.55	1.50	54, 55
Zn + ^{4}He	60	8.41	1.46	54, 55
Zr + ^{4}He	80	9.07	1.45	55
Nb + ^{4}He	82	8.99	1.43	55
Mo + ^{4}He	84	7.19	1.45	55
Ag + ^{4}He	94	9.52	1.47	55
Sn + ^{4}He	100	9.43	1.40	55
Ta + ^{4}He	146	10.65	1.44	55
Au + ^{4}He	158	11.04	1.46	55
Pb + ^{4}He	164	11.10	1.45	55
Bi + ^{4}He	166	11.06	1.44	55
Th + ^{4}He	180	11.13	1.40	55
Be + ^{12}C	24	6.42	1.47	58
C + ^{12}C	36	5.99	1.31	58
Al + ^{12}C	78	7.67	1.45	58
Fe + ^{12}C	156	8.62	1.41	58
Ni + ^{12}C	168	8.72	1.41	58
Cu + ^{12}C	174	8.99	1.43	58
Ag + ^{12}C	282	10.08	1.43	58
Sn + ^{12}C	300	10.09	1.40	58
Ta + ^{12}C	438	11.05	1.41	58
Au + ^{12}C	474	11.43	1.41	58
Be + ^{16}O	32	7.04	1.53	58
C + ^{16}O	48	6.83	1.42	58
Al + ^{16}O	104	8.23	1.49	58
Fe + ^{16}O	208	8.82	1.39	58
Ni + ^{16}O	224	9.36	1.46	58
Cu + ^{16}O	232	9.45	1.45	58
Ag + ^{16}O	376	10.12	1.39	58
Sn + ^{16}O	400	10.04	1.35	58
Ta + ^{16}O	584	11.12	1.36	58
Au + ^{16}O	632	11.92	1.43	58
Au + ^{16}O	632	11.84	1.42	58

[a] Low energy deuteron data (Refs. 20, 21, 45, 47, and 48) are not included in the least-squares analysis (Table III) and Figs. 12 and 13.

TABLE III. Radii obtained by least-squares analysis.

Nuclide	Radius (fm) [a]
^{1}H	1.443 ± 0.059
^{2}H	2.187 ± 0.078
^{3}He	3.506 ± 0.139
^{4}He	2.534 ± 0.078
$A \geq 6$	$(1.416 \pm 0.008)A^{1/3}$

[a] Uncertainties given are the standard deviations of the mean obtained with equal weights for each value of R_0 in Tables I and II.

of Z_1Z_2 and is quite well grounded. Similarly, the solid line representation of r_e seems to be rather well established. Data from Table IV have been omitted from Fig. 14 because they are considered to be more subject to the possibility of systematic errors. Nevertheless, these data points are consistent with the solid curve in Fig. 14 with the important exception of three points from Kr projectiles. We will return to this point.

Wong[7] and others[18] have pointed out that r_0 and r_e (as calculated from the real part of an optical potential) can be expected to decrease significantly with increasing Z_1Z_2. It is interesting to note that the constancy of r_0 with Z_1Z_2 is distinctly at variance with this expectation. The values of r_e do indeed decrease with Z_1Z_2 but at a significantly lower rate than calculated from an optical model with nonvarying parameters. (See the dashed curves in Figs. 13 and 14.) We have used the following set of Woods-Saxon parameters: $V_0 = -40.0$ MeV, $a = 0.50$ fm, $r_0 = 1.20$ fm, for all projectiles. The same calculated trend[18] results from a more detailed interaction potential $V(R)$ of the form

$$V(R) = \int V_1(\vec{R}_1)\rho_2(\vec{R} - \vec{R}_1)d^3\vec{R}_1 + Z_1Z_2e^2/R\,,$$

where $V_1(\vec{R}_1)$ is the real part of the single-nucleon potential for the first nucleus and $\rho_2(\vec{R} - \vec{R}_1)$ is the nucleon density in the second nucleus.

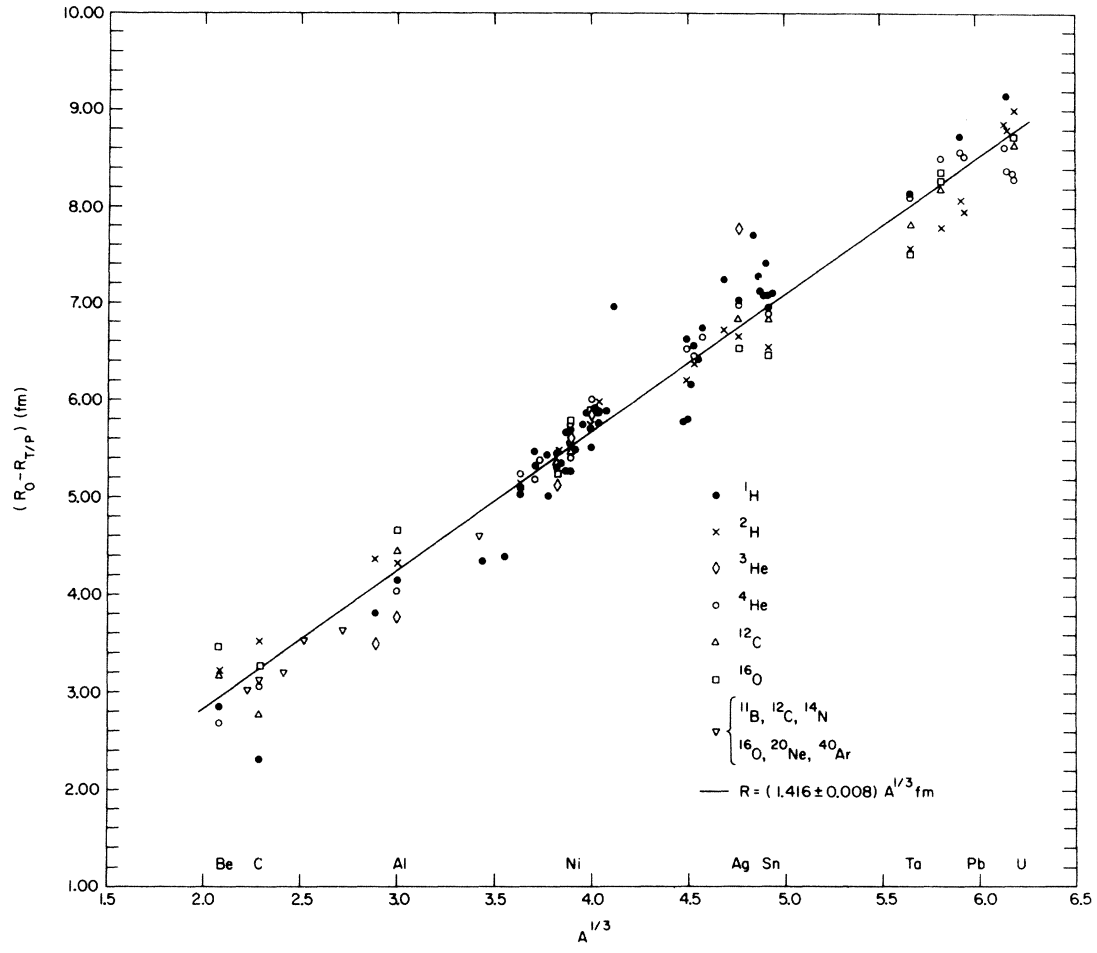

FIG. 12. Radius of target or projectile ($R_0 - R_{T/P}$) versus $A^{1/3}$. Smooth curve is for $R = 1.41A^{1/3}$ fm. Symbols correspond to the following projectiles: ●, ^{1}H; ×, ^{2}H; ◇, ^{3}He; ○, ^{4}He; △, ^{12}C; □, ^{16}O; and ▽ for ^{238}U targets.

TABLE IV. The parameter $\overline{E}_0$ from partial reaction cross sections measured at low energies.

Reaction	Energy span in c.m. (MeV)	Z_1Z_2	$\overline{E}_0$ (MeV)	r_e (fm)	Ref.
^{72}Ge(^{84}Kr, xn)	147–169	1152	150.2	1.29	59
^{116}Cd(^{40}Ar, $5n$)^{151}Dy	114–132	864	112	1.34	60
^{116}Cd(^{84}Kr, xn)	210–220	1728	209	1.29	59
^{164}Dy(^{40}Ar, $4n$)^{200}Po	130–141	1188	129	1.49	61
^{164}Dy(^{40}Ar, $4n$)^{200}Po	130–141	1188	135	1.43	62
^{195}Pt(^{14}N, $4n$)^{205}At	60–64	546	61	1.57	63
^{142}Nd(^{10}B, $3n$)^{149}Tb^{g}	33–41	300	36.5	1.61	64
^{197}Au(^{4}He, $2n$)^{199}Tl	20–26	158	20.3	1.51	65
^{197}Au(^{12}C, $3n$)^{206}At	53–59	474	51.5	1.63	66
^{197}Au(^{14}N, $4n+p3n$)^{207}At	63.5–68.5	553	64.0	1.51	66
^{205}Tl(^{16}O, $3n$)^{218}Ac	75–79	648	76	1.46	67
^{232}Th(^{22}Ne, $4n$)^{250}Fm	92-101	900	91	1.59	68
^{248}Cm(^{13}C, $4n$)^{257}No	61–68	576	61	1.43	69
^{239}Pu(^{18}O, $4n$)^{253}No	79–84	752	78	1.55	70
^{242}Pu(^{12}C, $4n$)^{250}Fm	60–68	564	60	1.59	71
^{242}Pu(^{18}O, $4n$)^{256}No	76–86	752	78	1.57	72
^{242}Pu(^{22}Ne, $4n$)^{260}Kh	99–104	940	99	1.51	73
^{232}Th(^{84}Kr, X)	337–358	3240	333	1.33	74
^{233}U(^{12}C, $3n$)^{242}Cf	57.7–60.4	552	58	1.62	75
^{244}Cm(^{13}C, $4n$)	63.5–72.5	576	61	1.58	69
^{246}Cm(^{12}C, $4n$)^{254}No	65–69	576	62	1.56	69
^{246}Cm(^{13}C, $4n$)^{255}No	63–69	576	63	1.53	69
^{248}Cm(^{12}C, $4n$)^{256}No	63–68	576	61.5	1.57	69
^{248}Cm(^{13}C, $4n$)^{257}No	61–67	576	61.5	1.56	69
^{197}Au(^{19}F, $3n$)^{213}Ra	74–86	711	75.5	1.60	76
^{209}Bi(^{84}Kr, X)	308.2–349.6	2988	304.8	1.37	77

Let us now reverse the direction of the discussion and turn to predictive aspects. Suppose one wished to estimate the total reaction cross section for a particular case, i.e., ^{208}Pb + ^{40}Ar. We would use Eq. (2) with a spectrum of E_0 values from $\overline{E}_0 - \Delta$ to $\overline{E}_0 + \Delta$ (not necessary for $E > 1.2E_0$). We would obtain r_e (or $\overline{E}_0$) from the solid line in Fig. 14 and r_0 (or R_0) from Table III as explained in the text. We would use $\hbar\omega_0 = 4.0$ MeV and $\Delta = 3.0$ MeV. For energies of about $\overline{E}_0$ and higher, we would expect to obtain a rather accurate prediction of σ_R (see Figs. 9–11).

The high values of the interaction barrier in Kr reactions are particularly interesting. Three of the four values of r_e for Kr beams (Table IV) are significantly smaller than that indicated by the solid curve in Fig. 14. This may signal an important new effect, enhanced Coulomb barriers for collisions between very heavy ions. However, we must note that these data points arise from partial reaction cross sections as described in the discussion of Table IV. The assumption of constancy of σ_i/σ_R may not be correct. For the present, it would seem best to use values of $\overline{E}_0$ from the solid curve, but one must recognize that this curve may indeed be altered as more data are obtained for high Z_1Z_2 (or for very heavy projectiles). More experimental information is certainly required to clarify this point.

B. Incident energies below barrier $E \lesssim \overline{E}_0$

As mentioned previously, there are very few reaction systems[42-44] for which experimental values of σ_R are known at energies below the barrier $E < \overline{E}_0$. We have, in fact, given low weight to those determinations at low energy in the parameter searches described so far. At low energies the magnitude of σ_R is very sensitive to each of the three parameters $\hbar\omega_0$, $\overline{E}_0$, and Δ as shown in Figs. 3, 4, and 7. Therefore, we can expect the fitting procedure to be very delicate here and hence the experimental data must be accurate and extensive. There are rather extensive data at low energies for 11 reaction systems; in this section we explore the fit of calculation to experiment for these systems.

In Table I we presented best-fit values of r_e, r_0, and Δ for 29 reaction systems. Low energy ($E \lesssim \overline{E}_0$) data were given small weight in these parameter determinations. The systematics of r_e and r_0 are

clearly shown in Figs. 13 and 14 and fixed values of $\hbar\omega_0$ (4.0 MeV) and Δ (3.0 MeV) give excellent fits at higher energies, $E \gtrsim \bar{E}_0$. The first question we have asked concerning the low-energy data is: "Can we get good fits to the low energy data by allowing more freedom in only the spectrum of barrier heights (i.e., r_e and Δ)?" We used a least-squares search routine[80] to determine the best values of r_e and Δ with $\hbar\omega_0$ and r_0 fixed at 4.0 MeV and 1.41 fm, respectively. The best-fit values of the parameters are given in Table V and the fits are shown in Figs. 15 and 16. For the ^{2}H and ^{4}He reactions slightly lower values of both $\bar{E}_0$ and Δ (compared to Table I) lead to rather good fits over the whole energy span. For the ^{1}H and ^{6}Li reactions good fits cannot be obtained at all energies with only r_e and Δ as free parameters. It is also apparent from Figs. 15 and 16 that each reaction type has its characteristic shape for energies less than $\bar{E}_0$. We conclude that the reaction systems at low energies are reflecting individualistic characteristics of the interaction barriers, and a simple representation of the potential with only two free parameters is inadequate.

The parabolic barrier approach as described has, of course, a total of four parameters, r_e, Δ, r_0, and $\hbar\omega_0$. The parameter r_0 seems to be heavily anchored at a value of 1.416 fm and is, in fact, not very important at low energies. (See Fig. 2.) There remain the parameters r_e, Δ, and $\hbar\omega_0$ and we have made a least-squares search with these three as free parameters. Indeed, very good fits were obtained for all energies for all 11 reactions. The best-fit parameters are listed in the last three columns in Table V.

The best-fit values of Δ, $\hbar\omega_0$, and r_e given in Table V do not vary in a simple way. The average values are very close to those we recommend for calculating σ_R at higher energies ($E \gtrsim \bar{E}_0$). However, the individual values differ significantly from the "average" behavior. For ^{4}He the values

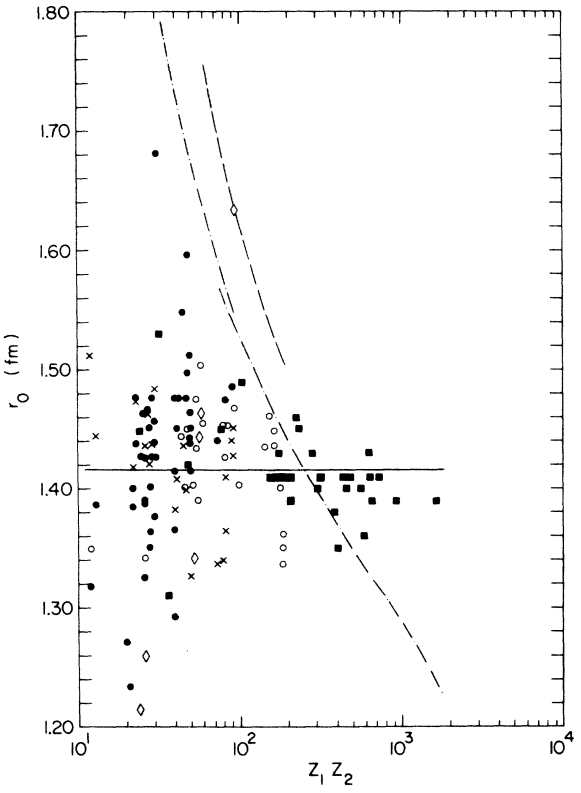

FIG. 13. The radius parameter r_0 versus Z_1Z_2. Points are from experiment as follows: ●, ^{1}H; ×, ^{2}H; ◇, ^{3}He; ○, ^{4}He; heavier projectiles, ■. The solid line is for r_0 = 1.416 fm. (See Fig. 12). Dashed curves were calculated with an effective potential [Eq. (4)] for s waves with parameters defined in Fig. 1, (a) —·— for ^{1}H for $Z_1Z_2 \leq 92$; and for $A \geq 6$ for $Z_1Z_2 \geq 92$, (b) — — for ^{3}He and ^{4}He. The calculated curves are somewhat different for each projectile, as indicated for H and He, but all follow the trend shown. Nuclear radii for ^{1}H, ^{2}H, ^{3}He, and ^{4}He are given in Table III.

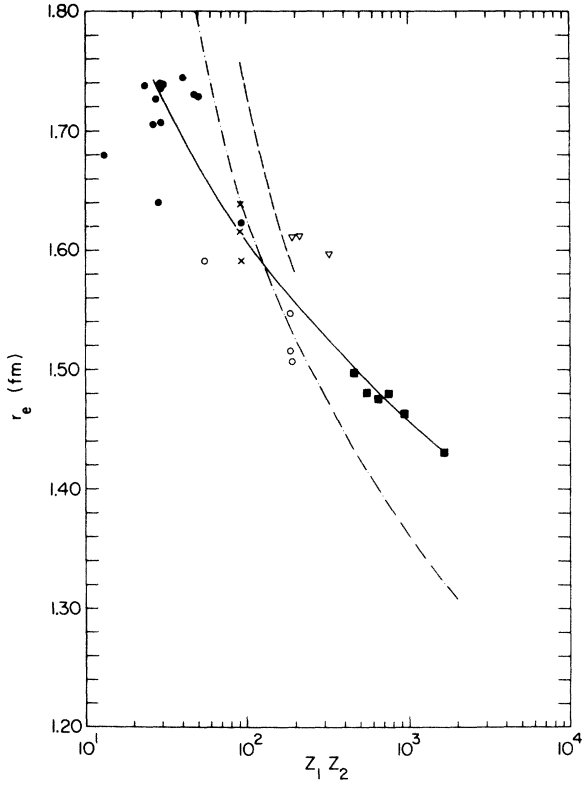

FIG. 14. The parameter r_e versus Z_1Z_2 [see Eqs. (6) and (7)]. Symbols are as follows: ●, ^{1}H; ×, ^{2}H; ○, ^{4}He; ■, ^{238}U targets; ▽, ^{32}S. Solid curve is drawn by eye through the points. Dashed curves were calculated from an effective potential (see Fig. 13), (a) —·— for ^{1}H for $Z_1Z_2 \leq 92$; and for $A \geq 6$ for $Z_1Z_2 \geq 92$. (b) — — for ^{3}He and ^{4}He.

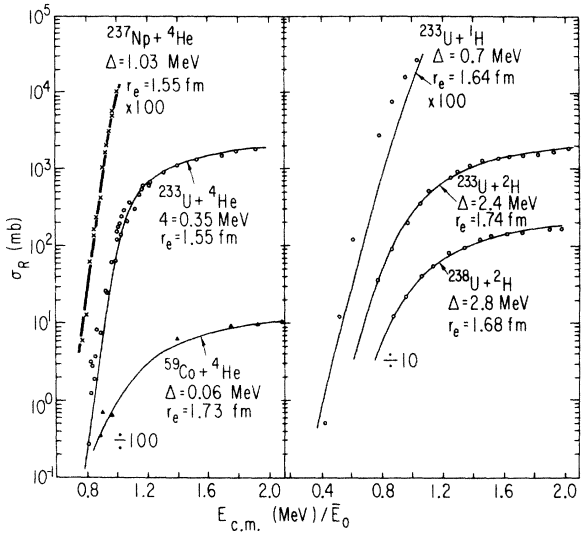

FIG. 15. Calculated curves and experimental points for σ_R vs $E/\bar{E}_0$ for several reactions. In the calculation values of r_0 and $\hbar\omega_0$ were fixed at 1.41 fm and 4.0 MeV, respectively. Best-fit values of r_e and Δ for each reaction are indicated. Only the lower energy region is shown for ^{233}U + ^{1}H.

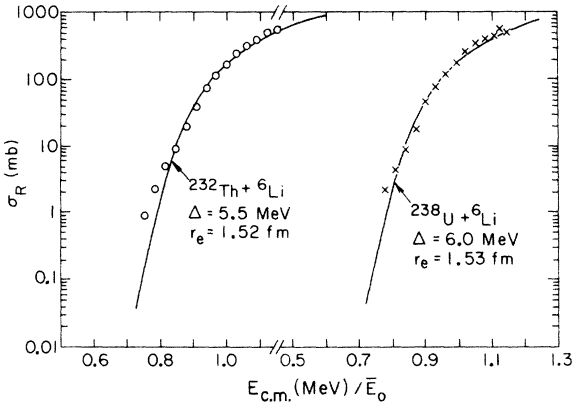

FIG. 16. Calculated curves and experimental points for σ_R vs $E/\bar{E}_0$ for the reactions (Ref. 43) of ^{6}Li with ^{232}Th and ^{238}U. In the calculation values of r_0 and $\hbar\omega_0$ were fixed at 1.41 fm and 4.0 MeV, respectively. Best-fit values of parameters r_e and Δ are indicated.

of both Δ and $\hbar\omega_0$ seem to be ≈3 MeV. For ^{1}H the spectrum of barrier heights seems to be particularly wide (i.e., large values of both $\bar{E}_0$ and Δ). For ^{6}Li and ^{2}H reactions the barrier spectrum seems to be particularly soft or penetrable (i.e., very large values of $\hbar\omega_0$ and/or Δ). These individualistic characteristics of the interaction barriers are very interesting and they certainly merit further study.

With these results in mind, the question arises: "What is the best way to calculate total reaction cross sections at low energies ($E \lesssim \bar{E}_0$)?" We recommend the prescription described in Sec. IV A unless data at low energies are available for a very similar reaction system. If such data are available, then a local parameter set (such as one of those in Table V) is probably preferable.

One should note that each of the reaction systems in Table V has obvious special characteristics, e.g. deformed target, ^{238}U; loosely bound projectile, ^{2}H or ^{6}Li; tightly bound projectile, ^{4}He. The parameter set which has the broadest base of comparison to measured reaction cross sections seems best to us at this time. As more data become available, new values of r_0 and r_e can easily be obtained as described above and the smooth

TABLE V. Barrier parameters from cross sections measured at very low energies.

		Two free parameters [a]			Three free parameters [b]		
Reaction	Ref.	Energy span $E/\bar{E}_0$	r_e (fm)	Δ (MeV)	r_e (fm)	Δ (MeV)	$\hbar\omega_0$ (MeV)
^{233}U + ^{1}H	19	0.44–1.04	1.64	0.7	1.31	6.4	2.3
^{233}U + ^{2}H	46	0.77–2.02	1.74	2.4	1.75	1.8	4.9
^{238}U + ^{2}H	46	0.88–1.97	1.68	2.8	1.68	2.6	4.4
^{59}Co + ^{4}He	52	0.90–2.76	1.73	0.06	1.75	0.8	3.4
^{208}Pb + ^{4}He	42,44	0.78–1.02	1.54	0.34	1.45	3.1	3.2
^{209}Bi + ^{4}He	42,44	0.77–1.00	1.53	0.25	1.47	2.9	3.1
^{233}U + ^{4}He	42,53	0.67–1.92	1.55	0.35	1.51	3.0	3.1
^{238}U + ^{4}He	6,42,53	0.67–1.85	1.52	0.64	1.50	3.2	2.8
^{237}Np + ^{4}He	56	0.78–1.00	1.55	1.03	1.46	3.2	3.5
^{232}Th + ^{6}Li	43	0.76–1.15	1.52	5.5	1.54	3.2	7.2
^{238}U + ^{6}Li	42,43	0.78–1.14	1.53	6.0	1.57	3.0	7.2

[a] The best-fit parameters were obtained by a free search least-squares routine with $\hbar\omega_0$ and r_0 fixed at 4.0 MeV and 1.41 fm. (See Ref. 80.)

[b] The best-fit parameters were obtained by a free search least-squares routine with r_0 fixed at 1.41 fm. (See Ref. 80.)

curves in Figs. 13 and 14 can be appropriately modified.

C. Comparisons with other models

A real parabolic potential barrier is clearly an oversimplification of the complicated interaction between charged nuclei. Oversimplification has the obvious advantage of reducing the number of parameters which describe the interaction barrier. However, the values of the parameters (obtained by fitting experimental data) may be distorted to varying degrees by nuclear properties that were ignored in the model.

Figure 13 shows values of r_0 and also a comparison to r_0 calculated from the real part of an optical potential (see caption of Fig. 1). The points from experiments show essentially a normal statistical distribution about a constant value of $r_0 = 1.416$ fm. If one separates the points for heavy ion projectiles for example, a slight decrease of r_0 with Z_1Z_2 might be indicated. Nevertheless, this change of r_0 with Z_1Z_2 is probably $\lesssim \frac{1}{5}$ of that calculated from the real part of an optical potential.[81] In this treatment the complex or absorptive part of the nuclear potential is not explicit but implicitly it is taken to be large for $R < R_0$ and small for $R > R_0$. It is possible that the absorptive or imaginary potential becomes weaker or less effective in the nuclear surface with decreasing Z_1Z_2. Such an effect would appear as a reduction in r_0 as deduced from Eq. (2).

The values of r_e in Fig. 14 do indicate a clear decrease with Z_1Z_2 as expected from the real part of an optical potential.[81] It appears that this decrease is significantly less rapid than expected. We have drawn one curve through points from different projectiles. As more data become available, it may turn out that each projectile behaves somewhat differently and this trend may therefore be modified.

Extrapolation of the solid lines in Figs. 13 and 14 would give $r_e \lesssim r_0$ for high Z_1Z_2. Strict interpretation of such a result would imply an interaction barrier higher than the Coulomb barrier between hard spheres in contact. Such an effect may, of course, occur but since we have employed such a simple potential (with no explicit absorptive term, no velocity dependence, etc.) we would not cite these figures as strong evidence.

In sum, we would caution against overinterpretation of the magnitudes of the potential parameters obtained here. However, we do feel that interpolation and extrapolation of these parameters provides a very good means of calculating total reaction cross sections.

ACKNOWLEDGMENTS

We appreciate helpful communications with Dr. C. Y. Wong. We thank Dr. J. Cumming for help with codes for matrix inversion and least-squares fitting.

---

*Work supported in part by the U. S. Atomic Energy Commission.

[1]G. Igo, Phys. Rev. 115, 1665 (1959).

[2]J. R. Huizenga and G. Igo, Nucl. Phys. 29, 462 (1962).

[3]R. M. Eisenberg and C. E. Porter, Rev. Mod. Phys. 33, 190 (1961).

[4]T. D. Thomas, Phys. Rev. 116, 703 (1959); P. W. Riesenfeldt and T. D. Thomas, Phys. Rev. C 2, 711 (1970).

[5]J. J. H. Menet, E. E. Gross, J. J. Malanify, and A. Zucker, Phys. Rev. C 4, 1114 (1971).

[6]V. E. Viola, Jr. and T. Sikkeland, Phys. Rev. 128, 767 (1962).

[7]C. Y. Wong, Phys. Lett. 42B, 186 (1972); Phys. Rev. Lett. 31, 766 (1973).

[8]See, for example: W. E. Frahn and R. H. Venter, Ann. Phys. (N.Y.) 24, 243 (1963); J. S. Blair, in *Lectures in Theoretical Physics* (Univ. of Colorado, Boulder, 1966), Vol. VIII C; Phys. Rev. 95, 1218 (1954); J. A. MacIntyre, K. H. Wang, and L. C. Becker, *ibid.* 117, 1337 (1960); J. Alster and H. F. Conzett, in *Proceedings of the Second Conference on Reactions between Complex Nuclei, Gatlinburg, Tennessee, 1960,* edited by A. Zucker, E. C. Halbert, and F. T. Howard (Wiley, New York, 1960), p. 175.

[9]See, for example: B. C. Robertson, J. T. Sample, D. R. Goosman, K. Nagatani, and K. W. Jones, Phys. Rev. C 4, 2176 (1971); J. Orloff and W. W. Daehnick, *ibid.* 3, 430 (1971); Y. Eisen, R. A. Eisenstein, U. Smilansky, and Z. Vager, Nucl. Phys. A195, 513 (1972); A. M. Friedman, R. H. Siemssen, and J. G. Cuninghame, Phys. Rev. C 6, 2219 (1972).

[10]N. T. Porile, in *Nuclear Chemistry,* edited by L. Yaffe (Academic, New York, 1968), Vol. I, p. 57; J. M. Blatt and V. F. Weiskoff, *Theoretical Nuclear Physics* (Wiley, New York, 1952); R. D. Evans, *The Atomic Nucleus* (McGraw-Hill, New York, 1955), Chaps. 8 and 14.

[11]B. Fernandez and J. S. Blair, Phys. Rev. C 1, 523 (1970).

[12]J. Rasmussen and K. Sugawara-Tanabe, Nucl. Phys. A171, 496 (1971).

[13]D. L. Hill and J. A. Wheeler, Phys. Rev. 89, 1102 (1953).

[14]P. H. Stelson and L. Grodzins, Nucl. Data A1, 21 (1965).

[15]The potentials were calculated using Eqs. (12) and (13) of Ref. 7.

[16]R. Beringer, Phys. Rev. Lett. 18, 1006 (1967); A. S. Jensen and C. Y. Wong, Phys. Rev. C 1, 1321 (1970);

Nucl. Phys. A171, 1 (1971); H. Holm and W. Greiner, Phys. Rev. Lett. 24, 404 (1970); H. Holm, W. Scheid, and W. Greiner, Phys. Lett. 29B, 473 (1969); H. Holm, Phys. Rev. C 7, 1716 (1973); P. W. Riesenfeldt and T. D. Thomas, Phys. Rev. C 2, 2448 (1970).

[17]Optical model potential ($V_0 = -40.0$ MeV, $r_0 = 1.2$ fm and $a = 0.50$ fm) for several target-projectile combinations give $\hbar\omega_0$ values of 3–6 MeV. For simplicity we use $\hbar\omega_0 = 4.0$ MeV.

[18]D. M. Brink, "Heavy ion reactions," Lectures at Orsay, March 1972 (unpublished); P. Colombani, J. C. Jacmart, M. Riou, C. Stephan, and J. Tys, Phys. Lett. 42B, 197 (1972).

[19]G. L. Bate and J. R. Huizenga, Phys. Rev. 133, B1471 (1964).

[20]K. Bearpark, W. R. Graham, and G. Jones, Nucl. Instrum. Methods 35, 235 (1965).

[21]K. Bearpark, W. R. Graham, and G. Jones, Nucl. Phys. 73, 206 (1965).

[22]P. J. Bulman, G. W. Greenlees, and M. J. Sametband, Nucl. Phys. 69, 536 (1965).

[23]P. J. Bulman and J. A. R. Griffith, Nucl. Phys. A111, 315 (1968).

[24]George F. Dell, W. D. Ploughe, and H. J. Hausman, Nucl. Phys. 64, 513 (1965).

[25]J. F. Dicello, G. Igo, and M. L. Roush, Phys. Lett. 23, 685 (1966).

[26]J. F. Dicello, G. J. Igo, and M. L. Roush, Phys. Rev. 157, 1001 (1967).

[27]E. J. Burge, Nucl. Phys. 13, 511 (1959).

[28]J. F. Dicello and G. Igo, Phys. Rev. 26, 488 (1970).

[29]M. Q. Makino, C. N. Waddell and R. M. Eisberg, Nucl. Phys. 68, 378 (1965).

[30]V. Meyer and N. M. Hintz, Phys. Rev. Lett. 5, 207 (1960).

[31]B. W. Shore, N. S. Wall, and J. W. Irvine, Phys. Rev. 123, 276 (1961).

[32]D. G. Montague, R. K. Cole, M. Q. Makino, and C. N. Waddell, Nucl. Phys. A199, 457 (1973).

[33]R. F. Carlson, R. M. Eisberg, R. H. Stokes, and T. H. Short, Nucl. Phys. 36, 511 (1962).

[34]C. Hojvat and G. Jones, Nucl. Instrum. Methods 66, 13 (1968).

[35]G. W. Greenlees and O. N. Jarvis, Proc. Phys. Soc. London 78, 1275 (1961).

[36]G. Igo and B. D. Wilkins, Phys. Lett. 2, 342 (1962); B. D. Wilkins and G. Igo, Phys. Rev. 129, 2198 (1963).

[37]R. E. Pollock and G. Schrank, Phys. Rev. 140, B575 (1965).

[38]W. T. H. van Oers, Phys. Rev. C 3, 1550 (1970).

[39]J. Wing and J. R. Huizenga, Phys. Rev. 128, 280 (1962).

[40]T. Sikkeland, Ark. Fys. 36, 539 (1967).

[41]H. H. Gutbrod, W. G. Winn, and M. Blann, Atomic Energy Commission Progress Report No. C00-3494-8, University of Rochester, 1973 (unpublished); Phys. Rev. Lett. 30, 1259 (1973); Nucl. Phys. A213, 267 (1973).

[42]H. Freiesleben and J. R. Huizenga, to be published.

[43]H. Freiesleben, G. T. Rizzo, J. R. Huizenga, and A. Prince, Atomic Energy Commission Progress Report No. C00-3496-29, University of Rochester, 1973 (unpublished).

[44]J. S. Lilley and M. Franey, Bull. Am. Phys. Soc. Ser. II, Vol. 18, No. 4, 605 (1973); A. R. Barnett and J. S. Lilley, Phys. Rev. C 9, 2010 (1974).

[45]U. Schmidt-Rohr and G. Wagner, Nucl. Phys. 71, 209 (1965).

[46]G. L. Bate, R. Chaudury, and J. R. Huizenga, Phys. Rev. 131, 722 (1963).

[47]K. Budzanowski and K. Grotowski, Phys. Lett. 2, 280 (1962).

[48]A. Budzanowski, L. Freindl, K. Grotowski, M. Rzeszutko, M. Slapa, J. Szmider, and P. E. Hodgson, Nucl. Phys. 49, 144 (1963).

[49]G. Igo and B. D. Wilkins, Phys. Lett. 3, 48 (1962).

[50]S. Mayo, W. Schimmerling, M. J. Sametband, and R. M. Eisberg, Nucl. Phys. 62, 393 (1965).

[51]R. Balcarcel and J. A. R. Griffith, Phys. Lett. 26B, 213 (1968).

[52]J. M. D'Auria, M. J. Fluss, L. Kowalski, and J. M. Miller, Phys. Rev. 168, 1224 (1968).

[53]J. R. Huizenga, R. Vandenbosch, and H. Warhanek, Phys. Rev. 124, 1964 (1961).

[54]A. Budzanowski, K. Grotowski, J. Kuzminiski, H. Niewodniczanski, A. Strazalkowski, S. Sykutowski, J. Szmider, and R. Wolksi, Nucl. Phys. A106, 21 (1968).

[55]G. Igo and B. D. Wilkins, Phys. Rev. 131, 1251 (1963).

[56]A. Fleury, F. H. Ruddy, M. N. Namboodiri, and J. M. Alexander, Phys. Rev. C 7, 1231 (1973); S. Y. Lin and J. M. Alexander (unpublished).

[57]E. Labie, J. Lega, P. Leleux, and P. C. Macq, Nucl. Phys. A205, 81 (1973).

[58]B. D. Wilkins and G. Igo, in *Proceedings of the Third Conference on Reactions between Complex Nuclei, Asilomar, California, 1963,* edited by A. Ghiorso, R. M. Diamond, and H. E. Conzett (Univ. of California Press, Berkeley, California, 1963).

[59]H. Gauvin, Y. LeBeyec, M. Lefort, and C. Deprun, Phys. Rev. Lett. 28, 697 (1972).

[60]J. B. Natowitz and J. M. Alexander, Phys. Rev. 188, 1734 (1969).

[61]T. Sikkeland, R. J. Silva, A. Ghiorso, and M. J. Nurmia, Phys. Rev. C 1, 1564 (1970).

[62]Y. LeBeyec, M. Lefort, and A. Vigny, Phys. Rev. C 3, 1268 (1971).

[63]T. D. Thomas, G. E. Gordon, R. M. Latimer, and G. T. Seaborg, Phys. Rev. 126, 1805 (1962); University of California Radiation Laboratory Report No. 9950, 1961 (unpublished).

[64]J. M. Alexander and G. N. Simonoff, Phys. Rev. 130, 2383 (1963).

[65]F. M. Lanzafame and M. Blann, Nucl. Phys. A142, 545 (1970).

[66]R. Bimbot, M. Lefort, and A. Simon, J. Phys. 29, 563 (1968).

[67]R. A. Gough, Ph.D. thesis, McMaster University, 1970 (unpublished).

[68]E. D. Donets, V. A. Karnaukhov, G. Kumpf, B. A. Gvozdev, and Yu. T. Chuburkov, Zh. Eksp. Teor. Fiz. 43, 11 (1962) [transl.: Sov. Phys.—JETP 16, 7 (1963)].

[69]T. Sikkeland, A. Ghiorso, and M. J. Nurmia, Phys. Rev. 172, 1232 (1968).

[70]V. L. Mikheev, V. I. Ilyushchenko, M. B. Miller, S. M. Polikanov, G. N. Flerov, and Yu. P. Kharitonov, Sov. J. At. Energy 22, 93 (1967).

[71]T. Sikkeland, S. G. Thompson, and A. Ghiorso, Phys. Rev. 112, 543 (1958).

[72]G. N. Flerov, S. M. Polikanov, V. L. Mikheev, V. I. Ilyushchenko, V. F. Kushniruk, M. B. Miller, A. M. Sukhov, and V. A. Shchegolev, Yad. Fiz. 5, 1186 (1967) [transl.: Sov. J. Nucl. Phys. 5, 848 (1967)].

[73]G. N. Flerov, Yu. Ts. Oganesyan, Yu. V. Lobanov, V. I. Kuznetsov, V. S. Druin, V. P. Perelygin, K. A. Gavrilov, S. P. Tret'yakova, and V. M. Plotko, Sov. J. At. Energy 17, 1046 (1964).

[74]R. Bimbot, H. Gauvin, Y. LeBeyec, M. Lefort, N. T. Porile, and B. Tamain, Nucl. Phys. A189, 539 (1972).

[75]T. Sikkeland, J. Maly, and D. F. Lebeck, Phys. Rev. 169, 1000 (1968); UCRL Report No. UCRL-17588 Rev., 1967 (unpublished).

[76]K. Vali, W. Treytl, and E. K. Hyde, Phys. Rev. 161, 1284 (1967).

[77]R. Bimbot and M. F. Rivet, Phys. Rev. C 8, 375 (1973).

[78]W. C. Hamilton, *Statistics in Physical Science* (Ronald Company, New York, 1960).

[79]This kind of result has, of course, been obtained before from many data analyses. It is interesting to note that the radius parameter from the Blair analysis of elastic scattering [1.414 + 0.042, quoted in D. D. Kerlee, J. S. Blair, and G. W. Farwell, Phys. Rev. 107, 1343 (1957)] is very nearly the same as that obtained by our analysis of σ_R. These two methods of analysis are, however, clearly not self-consistent.

[80]C. Y. Wong, private communication.

[81]Recently Krappe and Nix have calculated the interaction energy on the basis of a liquid drop model extended to include the finite range of nuclear forces. [H. J. Krappe and J. R. Nix, International Atomic Energy Agency Report No. IAEA-SM-174/12 (unpublished)]. The trend (and even the magnitude) of their values of r_0 and r_e is very similar to that calculated from the real part of an optical potential as shown in Figs. 13 and 14.